



HAL
open science

The phase field method-From fundamentals to practical applications in crystal growth

Aurélie Galfré, Xiaoqian Huang, Claudia Cogné, Françoise Couenne

► **To cite this version:**

Aurélie Galfré, Xiaoqian Huang, Claudia Cogné, Françoise Couenne. The phase field method-From fundamentals to practical applications in crystal growth. *Journal of Crystal Growth*, 2023, 620, pp.127334. 10.1016/j.jcrysgro.2023.127334 . hal-04259425

HAL Id: hal-04259425

<https://hal.science/hal-04259425>

Submitted on 26 Oct 2023

HAL is a multi-disciplinary open access archive for the deposit and dissemination of scientific research documents, whether they are published or not. The documents may come from teaching and research institutions in France or abroad, or from public or private research centers.

L'archive ouverte pluridisciplinaire **HAL**, est destinée au dépôt et à la diffusion de documents scientifiques de niveau recherche, publiés ou non, émanant des établissements d'enseignement et de recherche français ou étrangers, des laboratoires publics ou privés.



The phase field method – from fundamentals to practical applications in crystal growth

Aurélie Galfré *, Xiaoqian Huang, Françoise Couenne, Claudia Cogné

Université de Lyon, Université Claude Bernard Lyon 1, Laboratoire d'Automatique, de Génie des Procédés et de Génie Pharmaceutique (LAGEPP), UMR CNRS 5007, Domaine de la Doua, Villeurbanne, 69616, France

Abstract

In this paper, the phase-field method is described and used to model ice crystal growth that is studied in Chemical Engineering in the freezing or freeze-drying process. Two main partial differential equations are developed on the entire domain consisting of the liquid phase, the solid one, and the interface : (i) The Allen Cahn equation that describes the evolution of the phase field and (ii) the energy balance. In this paper, we explain how to preserve the thermodynamic consistency of the system to model quantitatively ice crystal growth, in particular concerning the choice of the free energy density. Several constitutive equations are used to model the specific properties of ice and water. Simulations are performed in 2D domain using Euler discretization for time to solve the system equations. A complete discussion is made concerning the "best way" to choose the main parameters for the simulation with respect to several physical properties like the interfacial tension of ice/liquid water or the equilibrium stability conditions. Finally, freezing simulations are presented and the potential of the phase field method in Chemical Engineering is discussed.

© 2011 Published by Elsevier Ltd.

Keywords: A1. Crystal morphology, A1. Interfaces, A1 Solidification, A2. Single crystal growth

1. Introduction

Some researches in Chemical Engineering focus on systems with moving interfaces between phases and with complex morphologies of the interface, such as emulsion, polymerization, mixing, and solidification processes (crystallization, freezing, drying, and freeze-drying). These moving boundary processes are very challenging to simulate.

In the case of solidification process, the models currently used in literature are based on i) a sharp interface as in the Stefan problem, ii) a coarse interface such the mushy zone representation or iii) a diffuse

*. Corresponding author : Aurélie Galfré aurelie.galfre@univ-lyon1.fr

interface with Phase Field Method (PFM), investigated in physics and material area.

The first and second approaches are not completely satisfactory. The major issue of the sharp interface treatment is about the numerical problems due to the discontinuity at the interface which has to be tracked by introducing a scalar function [1, 2, 3, 4]. The Stefan model is also only representative of stable solidification with a plane interface [5]. However, some sharp interface models of solidification are able to provide dendritic structures [6, 2]. In the mushy zone representation, a two-phase mixed region appears between the solid and liquid region that is considered as a porous medium. This representation can be developed either with two sharp interfaces [7] or by using discrete numerical approach with a cellular automaton [8]. The cellular automaton approach is based on discrete spatial cells. The type and state of each cell are known, and their dynamics depend on the cell states in its neighborhood. The interactions between cells make it easy to implement and computationally efficient. However, this approach lacks the connections between physical processes and parameters [9, 8].

The phase field method (PFM) was introduced in research activities about thirty years ago to investigate interfacial dynamic problems [10] in physics and material area. This method is based on thermodynamic rules which allow the modeling of physical phenomena during the phase transformation. It overcomes the difficulty of monitoring the solidification front, its creation and/or disappearance by providing a spatially diffuse interface along a finite width. This diffuse interface is represented through the scalar variable called phase field variable [11].

The bibliographical analysis shows a great interest of this method for material, metallurgical, and physics applications. In these fields, the method has been successfully applied to present the evolution of complex grain morphologies [12, 13], the splitting or coalescence of bubbles [12], realistic features of solid along solidification [10, 14, 15, 16, 17] and the microsegregation of species during crystal growth [12].

However, the phase field method is rarely developed in the Chemical Engineering area, especially due to the following limitations. Firstly, the method uses dimensionless equations, and the relations applied to physical parameters are not clearly explained [10, 15]. Secondly, the results presented in the literature are often merely qualitative. Only recently, the development of the thin interface limit theory [18, 19] has made it possible to use a numerical interface thickness several orders of magnitude larger than the physical interface thickness and to compare the results with experimental observations [17, 20].

The main objective of this work is to demonstrate the applicability of the phase field method to process simulation by investigating the solidification of a pure component (water). Crystal growth and patterns of ice and snow remain a large source of discussion and of computational works in literature [21, 22]. In the case of

ice crystal growing in undercooled water, morphology has been recently described in [23, 21]. Details will be given in section 3.3. In PFM field, several advanced works were done to represent the snowflake variety of patterns. The kinetic limited surface attachment effect and the ice anisotropy are both taken into account. The variety of snowflake patterns, its side-branching, and its growth kinetics in supersaturated atmosphere are even successfully reproduced in three-dimension [17, 11]. In the case of ice growing in undercooled liquid, both PFM study and experimental data were limited. The pioneering work of [10] enabled to show the ice pattern structure in a qualitative way and the influence of physics and computational parameters on ice growth. Several studies were recently conducted for binary systems, such ice growth from salted water [24] or ice growth from sugary water [25]. They reproduced the dendritic branching aspect of ice and retrieved the tip velocity of ice in a binary mixture environment. But to our knowledge, it lacks pure system investigation.

In this paper, the applicability of the PFM for the growth of ice in water is demonstrated by : (i) extending the phase field method currently used in physics to the Chemical Engineering field ; (ii) maintaining the thermodynamic consistency ; (iii) working with a system of real units, in order to ease the extension of the methodology to other pure components ; (iv) showing some quantitative simulation results of dendritic growth of crystal and comparing them to the Ivantsov solution and microscopic solvability theory [17, 26].

This paper is organized as follows : first, the basic principles are developed and explained ; in the second part, the model is applied to the crystallization of a pure component, namely water/ice solidification ; finally, simulations are carried out to investigate the influence of main physical parameters in order to conclude about the potential of the method in Chemical Engineering field.

2. Dynamical modeling of solidification

The system under consideration consists of a small volume V in which a pure material undergoes a phase transition between solid and liquid.

2.1. Phase Field Method

The PFM model is based on the Ginzburg–Landau free-energy functional of the biphasic system, the energy balance, and the so-called Allen-Cahn partial differential equations defined over the whole system. The latter will give the spatial evolution of the *phase field variable* denoted by ϕ . ϕ takes value 1 for the liquid state, 0 for the solid state, and intermediate continuous values in the diffuse interface (see Fig. 1). By using a diffuse interface and the parameter ϕ , the interface position is implicitly set.

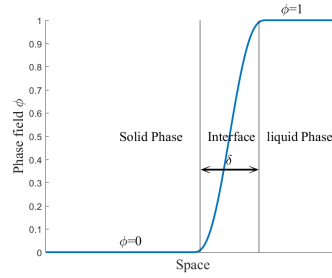


FIGURE 1. Diffuse interface : variable ϕ evolution throughout the interface

2.2. Thermodynamics description of the heterogenous pure system

The Ginzburg–Landau free-energy functional of a biphasic system for pure material is given by the relation (1) [27] :

$$F(\phi, T) = \int_v \left(f(\phi, T) + \frac{1}{2} \epsilon(\vec{n})^2 (\nabla\phi)^2 \right) dv, \quad (1)$$

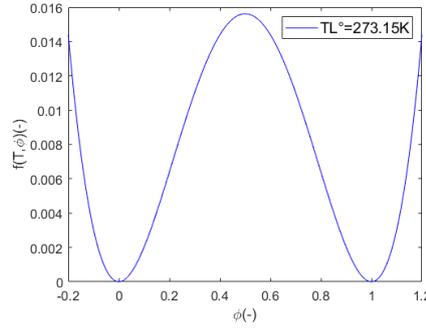
where T (K) is the temperature, $f(\phi, T)$ ($J.m^{-3}$) is the free energy density function associated with the Gibbs' equation. The quadratic term accounts for the free energy density of the diffuse interface where $\epsilon(\vec{n})$ is a positive constant related to the thickness δ (m) of the interface and its liquid/solid surface tension σ ($J.m^{-2}$) at melting temperature T_m [15, 27]. In order to manage the anisotropy of the system, we assume that $\epsilon(\vec{n})$ depends on the direction of the outer normal vector \vec{n} at the interface, which vector components are $(-\nabla\phi)$. The notation ∇ stands for the gradient.

Remark 1. In (1), the molar volume of the system is assumed to be constant since the molar volumes of liquid water and ice only differ by 3.5 % (maximal value) in the working area of temperature. The calculation was made by using property values (see 3.1).

Remark 2. Since the solidification takes place at constant pressure, the free energy functional F could be replaced by the "Gibbs energy" G in (1). The Gibbs energy G and the Helmholtz energy F only differ by a constant term. Since the minimization of the energy functional is used to lead the system solidification, either of these functions leads to the same conclusions

$f(\phi, T)$ has a double well structure whose minima correspond to the free energy density of each phase ($f_{liq}(T)$, $f_{sol}(T)$ for liquid and solid phase respectively). It is built by using an interpolating function $p_\phi(\phi)$ and a double well function $g_\phi(\phi)$.

$$f(\phi, T) = f_{sol}(T) + (f_{liq}(T) - f_{sol}(T)) p_\phi(\phi) + \frac{1}{4a} g_\phi(\phi) \quad (2)$$

FIGURE 2. Dimensionless density function $\tilde{f}(\phi, T)$ at T_m

The bump size of the free energy density for $0 < \phi < 1$ is controlled by the parameter a (m^3/J) in Eq.(2). In fig.2, the dimensionless free energy density $\tilde{f}(\phi, T) = f(\phi, T)a$ is plotted versus ϕ . Both a and ϵ are related to the interfacial energy and thickness. The choice of the polynomials functions and parameter a have to be carefully done to guarantee the thermodynamics consistency of the whole system [27] (see section 3.2 for our study case).

2.3. Dynamical model in two dimensions

The set of governing equations comprises the Allen-Cahn equation (3) and the energy conservation (4) as follows [27] :

$$\tau \frac{\partial \phi}{\partial t} = - \frac{\delta F(\phi, T)}{\delta \phi} \quad (3)$$

$$\frac{\partial u(s, \phi)}{\partial t} = \nabla(\lambda \nabla T) \quad (4)$$

where τ is the kinetic positive mobility coefficient and $\frac{\delta F}{\delta \phi}$ is the variational derivative of F with respect to ϕ . The energy balance is expressed using the internal energy density $u(s, \phi)$ ($J.m^{-3}$) as in [27]. This balance can also be written with respect to temperature (see below eq. (7)).

As properties are continuous throughout the interface, the interpolating function $p_\phi(\phi)$ is used to represent their evolution. The internal energy density $u(s, \phi)$ ($J.m^{-3}$) and the thermal conductivity $\lambda(\phi, T)$ are thus defined according to (5).

$$X = X_{sol} + p_\phi(X_{liq} - X_{sol}) \text{ for } X = u, \lambda \quad (5)$$

For pure material, the latent heat of fusion $L(T) = u_{liq} - u_{sol}$ is assumed to be constant in the working range of temperature since the maximal error committed is lower than 1% (energy densities calculations

made by using water and ice state equations from [28]). The relations $u_{liq} - u_{sol} \simeq L$ and $f_{liq}(T) - f_{sol}(T) \simeq \frac{L(T_m - T)}{T_m}$, with the latent heat of fusion L at melting point T_m , are commonly used [15] for calculation of properties. It facilitates the thermodynamics computation of the system and avoids time-consuming computations. The expanded final set of PFM equations becomes :

$$\tau \frac{\partial \phi}{\partial t} = -\frac{L(T_m - T)}{T_m} \frac{\partial p_\phi}{\partial \phi} - \frac{1}{4a} \frac{\partial g_\phi}{\partial \phi} + \nabla \cdot (\epsilon^2 \vec{n}) \nabla \phi \quad (6)$$

$$\frac{\partial T}{\partial t} = -\frac{L}{C_{vsol}} \frac{\partial p_\phi}{\partial t} + \frac{1}{C_{vsol}} \nabla T \nabla \lambda_{(\phi, T)} + \frac{\lambda_{(\phi, T)}}{C_{vsol}} \nabla^2 T \quad (7)$$

where C_{vsol} is the specific heat constant of solid phase in $J.m^{-3}.K^{-1}$.

2.3.1. Dimensionless model

To proceed further, the governing equations (6), (7) are rewritten in dimensionless form and applied in 2D spacial domain. As in [27], we introduce the length scale L_c representative of the size of the domain and use the time constant $\frac{L_c^2}{\kappa_{liq}}$ as the time reference scale with the thermal diffusivity of the liquid κ_{liq} ($m^2 s^{-1}$) at its initial temperature T_{liq}^0 . The energy density of the Allen-Cahn equation is rewritten in its dimensionless form with the bump a as in [15, 27, 29]. The dimensionless variables are :

$$\tilde{x} = \frac{x}{L_c}, \quad \tilde{y} = \frac{y}{L_c}, \quad \tilde{t} = \frac{t}{\frac{L_c^2}{\kappa_{liq}}}, \quad \tilde{T} = \frac{T - T_m}{T_{liq}^0 - T_m} \quad (8)$$

The dimensionless Allen-Cahn equation becomes :

$$\bar{\tau} \frac{\partial \phi}{\partial \tilde{t}} = \tilde{T} \alpha \frac{\partial p_\phi}{\partial \phi} - \beta \frac{\partial g_\phi}{\partial \phi} + \tilde{\nabla} \cdot (\tilde{\epsilon}^2 \tilde{\nabla} \phi) \quad (9)$$

with

$$\bar{\tau} = \frac{\tau a}{\frac{L_c^2}{\kappa_{liq}}}, \quad \tilde{\epsilon} = \frac{\sqrt{a} \epsilon(\vec{n})}{L_c}, \quad \alpha = \frac{L a (T_{liq}^0 - T_m)}{T_m}, \quad \beta = \frac{1}{4}$$

The notation $\tilde{\nabla}$ stands for the gradient with respect to dimensionless spatial variables.

The dimensionless energy equation becomes :

$$\frac{\partial \tilde{T}}{\partial \tilde{t}} = \frac{L}{C_{vsol}(T_m - T_{liq}^0)} \frac{\partial p_\phi}{\partial \tilde{t}} + \frac{\lambda(\phi, T)}{\kappa_{liq} C_{vsol}} \tilde{\nabla}^2 \tilde{T} + \frac{L_c}{\kappa_{liq} C_{vsol}} \tilde{\nabla} \lambda(\phi, T) \tilde{\nabla} \tilde{T}. \quad (10)$$

The thermal conductivity gradient is :

$$\tilde{\nabla} \lambda(\phi, T) = \frac{1 - p_\phi}{L_c} \frac{\partial \lambda_{liq}}{\partial \tilde{T}} \tilde{\nabla} \tilde{T} + \frac{p_\phi}{L_c} \frac{\partial \lambda_{sol}}{\partial \tilde{T}} \tilde{\nabla} \tilde{T} + \frac{\tilde{\nabla} p_\phi}{L_c} (\lambda_{liq}(T) - \lambda_{sol}(T)) \quad (11)$$

In PFM literature [10, 13], to simplify the system description, the melt and solid phases take the same properties for conductivity and heat capacity. Hence, the conductivity gradient $\tilde{\nabla} \lambda$ is not taken into account for the energy conservation formulation in many phase field models. To be as close as possible to a quantitative representation of the growth process, the temperature impact is added here for this gradient.

2.3.2. Anisotropy constitutive equation

To observe the microscopic features of the solid along its solidification, independent control of the anisotropy is included as in other works [24, 10] .

$$\epsilon(\vec{n}) = \epsilon(1 + \delta_a \cos(b_n \theta)) \quad (12)$$

where the parameter δ_a drives the strength of the anisotropy, b_n is the branches number of the crystal. θ is the angle between the interface normal vector (\vec{n}) and a given crystallographic direction. Its expression is given by :

$$\theta = \arctan\left(\frac{\nabla \phi_x}{\nabla \phi_y}\right) \quad (13)$$

3. Parameters of ice freezing

In this section, thermal and physical properties of ice and liquid water required for the model computations are detailed. Then, the polynomial forms of $p_\phi(\phi)$ and $g_\phi(\phi)$ as well as some choices in the thermodynamics model are specified. Finally, the phase field parameters, namely a , ϵ , τ , and the specific anisotropy constitutive function and pattern of ice are presented in this section.

3.1. Thermal and physical properties of liquid water and ice

At atmospheric pressure, thermophysical properties of liquid water and ice, namely thermal conductivity, heat capacity, density, latent heat and surface free energy, are listed in Table 1. All properties are functions

of temperature and are expressed by using a polynomial expression in order to make their computations easier in the simulation. Some of the polynomial functions proposed in Table 1 are built by using the state equations of ice and water proposed in [28]. The polynomial functions are valid in the temperature range (from 253K to 273K) .

TABLE 1. Properties of ice and water

Water			
Thermal conductivity (λ_{liq})	$W.m^{-1}.K^{-1}$	$0.57109 + 1.7625 \cdot 10^{-3}T - 6.7036 \cdot 10^{-6}T^2$	[30]
Density (ρ_{liq})	$kg.m^{-3}$	$1000.50 - 1.3781 \cdot 10^{-1}T - 2.3195 \cdot 10^{-2}T^2$	[28]
Heat Capacity (C_{vliq})	$J.kg^{-1}.K^{-1}$	$4208.4 - 3.6409 \cdot 10^{-1}T + 3.5508 \cdot 10^{-1}T^2$	[28]
Ice			
Thermal conductivity (λ_{sol})	$W.m^{-1}.K^{-1}$	$2.2196 - 6.2489 \cdot 10^{-3}T + 1.0154 \cdot 10^{-4}T^2$	[30]
Density (ρ_{sol})	$kg.m^{-3}$	$916.75 - 0.13073T$	[28]
Heat Capacity (C_{vsol})	$J.kg^{-1}.K^{-1}$	$2096.5 + 7.3034T$	[28]
Ice/water properties at 0°C			
Latent heat of fusion (L)	$J.m^{-3}$	$305.65 \cdot 10^6$	[28]
Surface free energy (σ)	$J.m^{-2}$	$2.85 \cdot 10^{-2}$	[31]
<i>with T (°C)</i>			

3.2. Thermodynamics consistency of the model

The Ginzburg–Landau free-energy functional F (1) has to be written in a thermodynamically-consistent manner to have a quantitative evolution of the system in transition. For this purpose, each term of the functional are discussed in the hereafter paragraphs.

3.2.1. Choice of polynomials $p_\phi(\phi)$ and $g_\phi(\phi)$

The density function $f(\phi, T)$ (2) needs to have, for all values of temperature T , local minima with respect to each phase, such as [32] :

$$\left. \frac{\partial f}{\partial \phi} \right|_{\phi=0} = \left. \frac{\partial f}{\partial \phi} \right|_{\phi=1} \quad \text{and} \quad \left. \frac{\partial^2 f}{\partial \phi^2} \right|_{\phi=0,1} > 0. \quad (14)$$

Besides, at equilibrium, the variational derivative of the Landau-Ginzburg functional (3) must be equal to 0, then, we need to check [15] :

$$\left. \frac{\partial f}{\partial \phi} \right|_{\phi=0,1} = 0. \quad (15)$$

Appropriate polynomial functions $p_\phi(\phi)$ and $g_\phi(\phi)$ are selected to make sure to have the desirable properties for $f(\phi, T)$. Several propositions were made in the literature [33]. Kobayashi [10] choose to use $p_\phi(\phi) =$

$\phi^2(32\phi)$ and $g_\phi(\phi) = \phi^2(1\phi)^2$ for the ice/liquid water system. In this case, the second derivative of the density function $f(\phi, T)$ according to ϕ (14) is positive only if the parameter a (see (2)) fulfills the additional condition ($|\frac{12aL(T_m T)}{T_m}| < 1$). Since the parameter a allows to manage the interfacial energy and thickness (see (17) and (18)), then this choice has been excluded to avoid any size limitation of the interface by the polynomial function choice. By using, $p_\phi(\phi) = \phi^3(6\phi^2 - 15\phi + 10)$ and $g_\phi(\phi) = \phi^2(1 - \phi)^2$, as proposed by [27, 15], the stability conditions (14), (15) are all fulfilled by fixing $a > 0$: these functions have been retained in the model formulation.

3.2.2. Phase field parameters

The parameters a and ϵ that appear in (1) are commonly related to the interface thickness δ and the surface free energy σ in literature [15, 27]. For this purpose, an one-dimensional solution of the isotropic form of (9) is established under equilibrium conditions [27]. This solution gives the shape of the variable ϕ in the diffuse interface [27] (the interface is located around $x = 0$).

$$\phi(x) = \frac{1}{2}(\tanh(\frac{x}{2\sqrt{2a\epsilon}}) + 1) \quad (16)$$

The approximated size of diffuse interface thickness δ is given by :

$$\delta = 2\alpha a^{1/2}\epsilon \quad (17)$$

By taking the reciprocal function of (16), we can determine the values of $-\delta/2$ and $+\delta/2$ for $\phi = 0.01$ and $\phi = 0.99$, respectively. In this case, $\alpha \simeq 7.48$. By using α , the thickness of the interface can be assessed for simulation.

The interfacial tension $\sigma(T_m)$ of ice/liquid water system and the phase field parameters a and ϵ are related by (18) [13, 27] :

$$\sigma(T_m) = \frac{\sqrt{2}\epsilon}{12\sqrt{a}} \quad (18)$$

This relation is found by using the Helmholtz free energy functional equation (1) associated with the one-dimensional solution of ϕ (16), evaluated at equilibrium conditions and expressed by the unit of surface area [34]. Notice that this last relation is established by using the commonly accepted convention $f_{liq}(T_m) = f_{sol}(T_m)$.

In practice, to use the model in a phenomenological way, the interfacial tension $\sigma(T_m)$ needs to be correctly reproduced in order to predict the interfacial properties. This parameter is thus a physical property

(see Table 2). Most authors do not fix the interface size but prefer to fix the dimensionless variable $\bar{\epsilon}$ at a low value in order to have an interface size to be less than L_c but large enough for computations. Consequently, $\bar{\epsilon}$ and L_c are computational parameters (see table 2). Typically, $\bar{\epsilon}$ takes values between 0.01 to 0.08 ([10, 18, 19]).

3.3. Ice patterns and anisotropy

In the case of ice crystal growing in undercooled water, the morphology diagram of nonequilibrium patterns was proposed in a wide undercooling range $0.1\text{C} < \Delta T < 30\text{C}$ [23, 21]. For a small undercooling (1C), a microscopic seed crystal tends to grow into the form of a simple circular disk. The basal surface structure of ice is maintained by the limited surface attachment kinetics. The growth of the disk edge is also limited by the diffusion of latent heat. As the undercooling increases ($\Delta T = 2\text{C}$), the disk growth becomes unstable, resulting in the formation of dendritic branching, and the basal faceting remains. The side branching occurrence is commonly explained by the Mullins–Sekerka instability theory [35]. For larger undercooling ($\Delta T = 4\text{C}$), unbranched needle-like structures appear, to branched needle-like structures ($\Delta T = 8\text{C}$), to platelets ($\Delta T = 10\text{--}30\text{C}$).

As previous works [10, 24], we added the six-fold symmetry of ice by fixing the branch number to 6; the anisotropy parameter δ_a varies following literature from 0.01 to 0.05. We fix it to 0.03 as in [24]. Finally, an uniformly distributed noise is added to produce side branching on the crystal. Indeed, in the absence of such noise and in the case of fine mesh spacing dx , it appears that dendrites in pure system tend to grow without side-branching to needle-like dendrites. Only small perturbations corresponding to thermal noise are responsible for the side-branching dendrites. Here, the noise is added in the dynamic term of the phase field equation (6), as proposed by [24].

$$\bar{\tau} \frac{\partial \phi}{\partial \bar{t}} = \bar{T} \alpha \frac{\partial p_\phi}{\partial \phi} - \beta \frac{\partial g_\phi}{\partial \phi} + \tilde{\nabla} \cdot (\bar{\epsilon}^2 \tilde{\nabla} \phi) + r\eta 16g_\phi(\phi) \quad (19)$$

where $r(x, y, t)$ is a random number between -1 to +1, and η is the disturbance intensity parameter of the phase field fixed to 0.03 after computational research. The maximum disturbance will occur at the interface when $\phi = 0.5$, and as we move further away from the interface, the disturbance gets smaller. The term $16g_\phi(\phi)$ is used to introduce the forced disturbance on the interface.

3.4. Kinetic constant τ

To achieve the appropriate interface kinetics, the problem is often reduced to the study of the macroscopic free boundary model which involves the following system of equations in the case of the solidification

process : the Stefan condition equation, the generalized Gibbs-Thomson equation, and the energy conservation equation (see [15, 18] for details). The parameter τ can be explicitly calculated by using the relation between the material parameters and the interface kinetic coefficient $1/\mu$ from the generalized Gibbs-Thomson equation (20) established for an isotropic interface :

$$T = T_m - \frac{\sigma T_m \zeta}{L} - v \frac{1}{\mu} \quad (20)$$

This relation links the interface temperature T , the normal ice growth rate v ($m.s^{-1}$) and the interface curvature ζ . The interface temperature T deviates from the equilibrium value T_m by two terms : the first is the capillary shift of the melting temperature (Gibbs-Thomson effect) ; the second is due to interface kinetics. Karma (1998)[18] related the interface kinetic $1/$ to the kinetic coefficient τ , by performing an asymptotic analysis of the phase field model equations in the case of the thin interface limit. The relation is :

$$\frac{1}{\mu} = \frac{a_1 L}{C_v} \left(\frac{\tau}{\lambda W} - a_2 \frac{W}{\kappa} \right) \quad (21)$$

where $a_1[-]$ and $a_2[-]$ are computational parameters depending of the choice of the polynomial functions and $\lambda = \frac{a_1 W}{d_0}$ and $W = a^{1/2} \epsilon$. If we assume that the temperature is constant in the interface, which is often called as the sharp interface limit [29], then the second term of (21) vanishes, and the kinetic coefficient τ is obtained by :

$$\bar{\tau} = \frac{\bar{\epsilon}^2 L \kappa_L}{\mu \sigma T_m} \quad (22)$$

By using this method, W and meshing dx have to be scaled small enough compared to the scale of dendrite pattern in order to converge to a reliable quantitative solution of the sharp-interface equations. Besides, some authors highlighted that simulations at smaller undercooling seemed to exhibit a dependence on the interface thickness[29].

For large undercooling, Langer et al. [36] and Shibkov [23] reported the tip-velocity v of an isolated dendrite of ice growing freely in a pure and undercooled liquid for different undercooling values. By using experimental data, rough values of $\frac{1}{\mu}$ and $\bar{\tau}$ from T_{liq} between -5 and -25C can be evaluated. They are reported in Table 2.

3.5. Model simulation

3.5.1. Numerical method and boundary conditions

The spatial 2D domain is discretized using $N \times N$ points. The explicit Euler method is used for time integration. The centered finite difference method is used to discretize gradient and divergence operators. Divergence is computed using a 9-points laplacian.

For the boundary conditions, since the system is isolated, there is no heat flux at boundaries. For this simulation, the germ (80 meshes) is located in the middle of the space under consideration.

3.5.2. Parameters of the simulation

TABLE 2. Simulation parameters

Definition	Parameter	Value(s)	Unity
Initial undercooling degree of temperature	$T_m - T_{liq}^0$	5, 10, 15	K
Dimensionless grid spacing	$d\tilde{x}$	0.02	[-]
Dimensionless time	$d\tilde{t}$	$5 \cdot 10^{-5}$	[-]
Mesh number in x-axis or y-axis direction	N	600	[-]
Mesh number of initial crystal nucleus diameter		80	
Bump size of the free energy density	a	$3.37 \cdot 10^{-7}$	m^3/J
Computational parameter	$\bar{\epsilon}$	0.06	[-]
Computation size	L_c	$1.3 \cdot 10^{-6}$	m
Energy gradient constant	ϵ	$1.39 \cdot 10^{-4}$	$J^{1/2} \cdot m^{-1/2}$
Kinetic constant of Allen-Cahn equation	$\bar{\tau}$	0.25	[-]
Capillarity diameter	d_0	$3.4 \cdot 10^{-10}$	m
Anisotropy factor for ϵ	δ_a	0.03	[-]
Branch number	b_n	6	[-]

Due to the large number of parameters, parameter assessment for phase field models is not straightforward. For a fixed set of physical parameters, several tests were made to have the better set of computational parameters (see table 2). Several sets of computational parameters ($\bar{\epsilon}$, L_c , $d\tilde{x}$, $d\tilde{t}$, δ) were tested. For each numerical test, we followed the method proposed by [26] to have a reasonable independence of computational parameters for the ice growth simulation. The following points have to be checked :

- The grid spacing $dx = L_c d\tilde{x}$ has to be much smaller than the interface thickness δ (calculated by (17)). Besides, the grid spacing dx/W ratio is about 0.3 to avoid spinning effect.
- To retrieve the results of the Gibbs Thomson relation (20) according to [18], the computational thickness W has to be fine enough in order to check $\frac{W}{d_0} \ll \kappa\tau/W^2$.
- To observe the crystal growth in an undercooled liquid temperature without large variation of its temperature for an isolated system, the simulation grid size has to be wide.

– Once $d\tilde{x}$ is chosen, the time step $d\tilde{t}$ has to be small enough to fulfill the Fourier stability criterium.

The selected simulation parameters for the water-ice system are shown in Table 2.

4. Results and discussion

4.1. Comparison

Figures 3, 4, 5 give snapshots at different times of the phase field $\phi(t, x, y)$ and the temperature field $T(t, x, y)$ for initial liquid temperature $T_{liq}^0 = -5^\circ C$, $T_{liq}^0 = -10^\circ C$ and $T_{liq}^0 = -15^\circ C$, respectively. Zooms of some snapshots are presented to evidence the crystal pattern. The figures are presented with real size of the crystals and real time.

At $t = 0ms$, one solid spherical germ is placed at the grid middle as shown in Figure 3. In Figures 3, 4, and 5, the typical hexagonal prism of ice is observed in the early stages of the crystal growth. This form remains for a longer time at low undercooling. In all cases, at some time, the crystal exhibits the formation of the first branch and side branches. At high undercooling, the crystal shows numerous side branching and the dendritic pattern of ice. The effect of heat conduction is also clearly evidenced on the temperature field as crystal growth progresses.

In Figure 6, three cross-sections of the phase field (in horizontal, vertical, and diagonal directions of the grid) are depicted for $T_{liq}^0 = -15^\circ C$. The number of points inside the interface is large enough in order to have an impact of the ϕ gradient on the interface orientation. It can be noticed that the interface number of meshes is around 20.

To compare our simulation results to experimental data [36, 23] and to the Ivantsov solution [37], we also compute the tip velocity v_{tip} (see Figure 7) of the crystal in growth in the following manner : we define the interface by the locus $\phi < 0.99$ and retrieve the dendrite tip position on the middle of x-axis, every 5000 steps of time [17]. In Figure 7, as expected, the crystal growth velocity depends on the undercooling conditions and physical properties of each phase. The steady state is quasi-achieved at the early stage of crystallization. At steady state, we confronted experimental data, the steady-state simulated tip velocity and the Ivantsov solution values for each undercooling condition (see Table 3). The Ivantsov equation [37] is a well-known relation used to calculate the tip velocity of a solid phase at constant temperature T_m which extends into an undercooled melt in diffusive conditions. Inside the melt the temperature drops and reaches far from the interface its asymptotic value T_{liq}^0 at steady state. The Ivantsov relation connects the Peclet number $Pe = v_{tip}R/2\kappa_L$ and the undercooling $\Delta = (T_m T_{liq}^0)C_{vL}/L$. Here, v_{tip} and R are the tip-velocity and

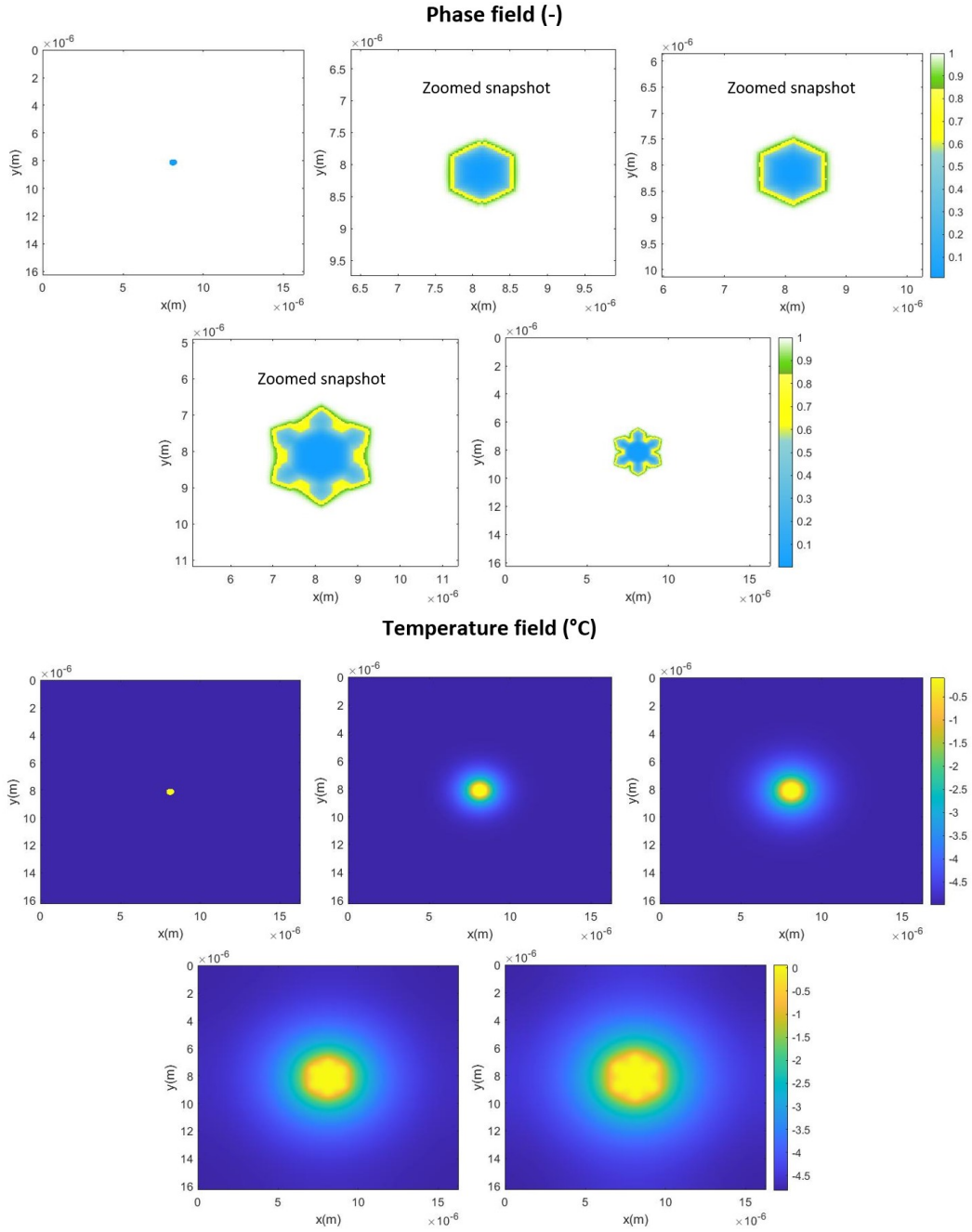


FIGURE 3. Simulation at $t = 0 \text{ ms}$, $t = 0.013 \text{ ms}$, $t = 0.027 \text{ ms}$, $t = 0.061 \text{ ms}$, $t = 0.13 \text{ ms}$, $t = 0.19 \text{ ms}$ for $T_{liq}^0 = -5^\circ\text{C}$

the tip-radius of a parabola interface, respectively, of the first branch. For the 2D case, in the case of dendritic growth :

$$\Delta = (\pi P_e)^{0.5} e^{P_e} \text{erfc}(P_e^{0.5}) \quad (23)$$

To use the Ivantsov solution, the tip radius R of the crystal needs to be calculated. To this end, the crystal edge and curvature of the crystal have been numerically obtained by adapting the function from [38]. The adequacy of the function can be checked with a circular geometry and at different sizes.

In Table 3, the numerical velocities are lower than the experimental ones. The values range is however respected. Whatever the undercooling degree, the tip velocity calculated with the Ivantsov solution is not in good agreement with the experimental data and the PFM simulated results. This can be resolved by : i) improving the radius tip calculation in the case of solid picture with a high branching degree ; ii) improving the simulation results. Indeed, the radius tip of the first branch in the PFM simulation pictures is perhaps different from the experimental one, i.e the form of the crystal is not totally quantitative in our simulations. In both cases, in order to improve the results of the study, relevant experimental data of the tip radius of ice and patterns are required to compare them with PFM simulation results.

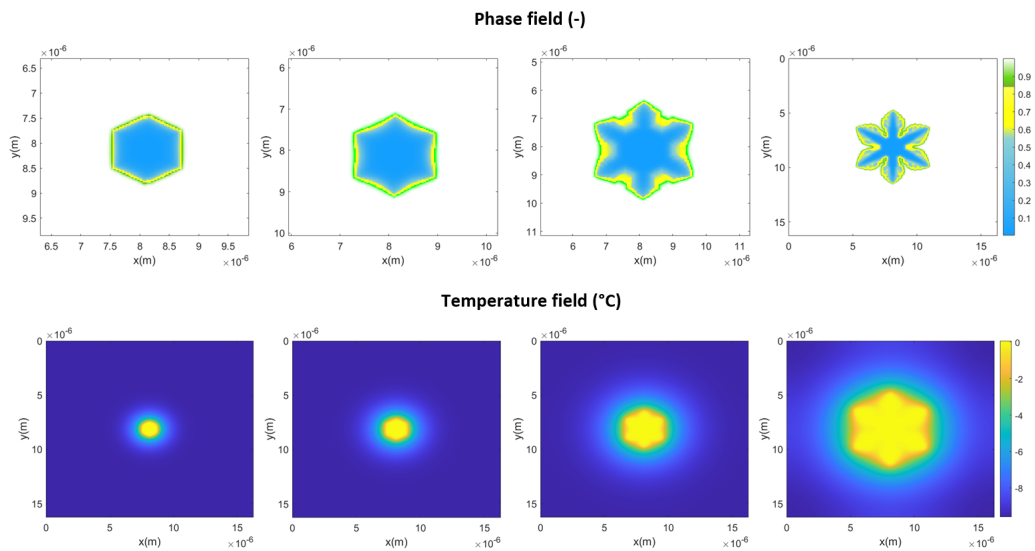


FIGURE 4. Simulation at $t = 0.013 \text{ ms}$, $t = 0.027 \text{ ms}$, $t = 0.068 \text{ ms}$, $t = 0.16 \text{ ms}$ for $T_{liq}^0 = -10^\circ\text{C}$

TABLE 3. Ice growth velocity comparison

Undercooling temperature (C)	Velocity (cm/s)	Method
5, 10, 15	0.8 ± 0.1 , 1.5 ± 0.1 , 4.4 ± 0.4	PFM simulation results
5, 10, 15	1.1 ± 0.1 , 2.6, 5.7	Experimental results [36, 23]
5, 10, 15	0.1, 0.6, 1.2	Ivantsov method [37]

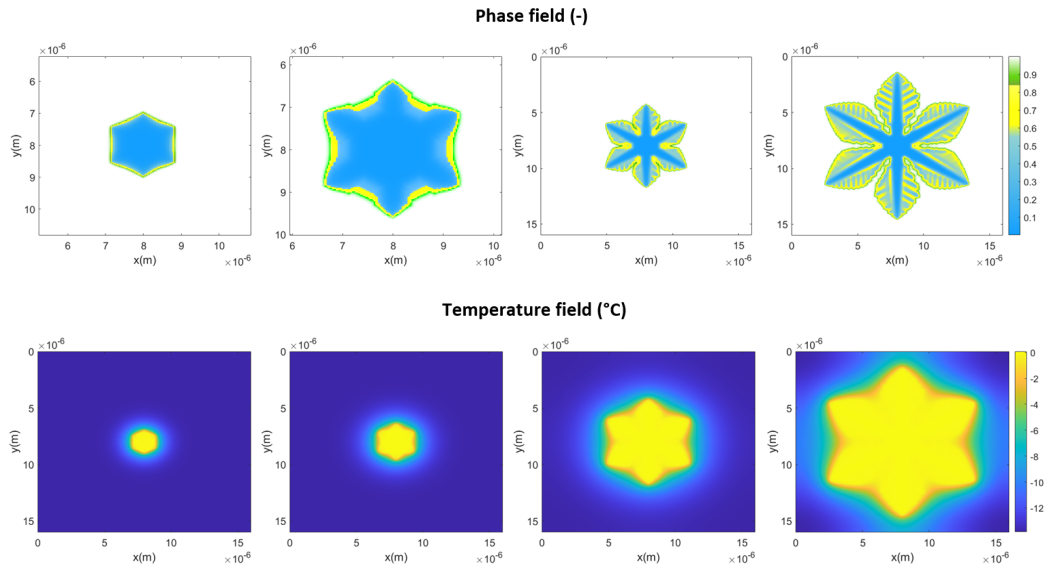


FIGURE 5. Simulation at $t = 0.013 \text{ ms}$, $t = 0.027 \text{ ms}$, $t = 0.08 \text{ ms}$, $t = 0.16 \text{ ms}$ for $T_{liq}^0 = -15^\circ\text{C}$

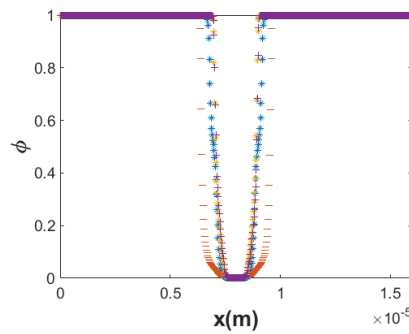


FIGURE 6. Several cross sections of the phase field (in horizontal *, vertical – and diagonal + of the grid) for $T_{liq}^0 = -15^\circ\text{C}$ and $t = 0.027 \text{ ms}$

4.2. Potential of the Phase field method application in the Chemical Engineering field

One major advantage of the phase field method is that the control of the interface and its anisotropy are included in the model formulation. The anisotropy function is empirically chosen in our case. We choose a classical one that is easy to implement. It can be noticed that some advanced studies in literature [17, 11, 39] employed an anisotropy function which enables to check the position of the first branch and side branching of snow in a quantitative manner.

Parameters (see section 3.2) are chosen to respect the thermodynamic consistency of the system. Numerical parameters (see 3.5.2) are also selected to limit the influence of the numerical method. It leads to simulating the system at microscale size to conserve a small but consistent interface width. As there are

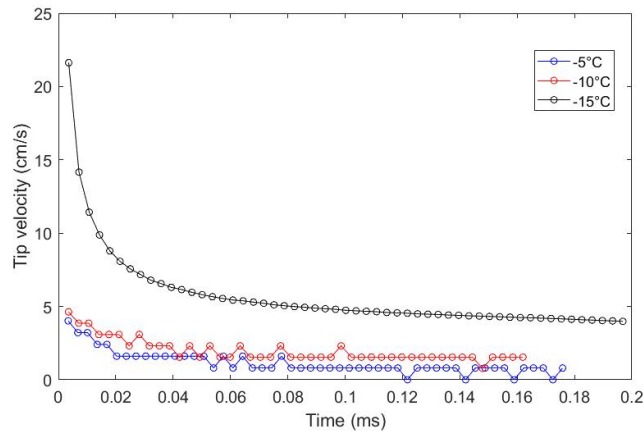


FIGURE 7. Tip velocity over time for each undercooling condition

properties gradients in the interface that needs to be correctly simulated, the point number in the interface is large and the computation of the system is time-consuming. These inconveniences limit the use of the phase field method in the Chemical Engineering field. In our opinion, phase field simulation can be a powerful tool to give local information about the macroscopic system as a snapshot in the field of Chemical Engineering. To expand the scope of application in Chemical Engineering, the model should be extended to binary system by taking into account mass transfer and binary equilibrium phase. A better computational method needs to be chosen to avoid time and space computation limitations. The parameters selection can also be performed by using the thin interface method [18] : it enables to work with a higher size of the interfacial thickness and can provide better quantitative results at low undercooling [29] for both the tip velocity and the solid patterns aspect.

5. Conclusion

The potential of the phase field method is a worthwhile goal in the Chemical Engineering field because it allows observing the formation of defects during ice growth such as anarchic ice, and solute incorporation,... As presented in this work, it is possible to develop a thermodynamically consistent model to simulate the kinetics and the facies of the interface. The example discussed in this article concerns dendritic solidification for ice-freezing applications. A large number of parameters of the model have been correlated to well-known properties of water, ice or ice/water equilibrium. Numerical parameters have been investigated to study the growth and the sidebranching. Using this model approach is very challenging in Chemical Engineering because it contains a great deal of known physics. The approach developed in this article concerning ice

growth could be easily extended to a binary system for crystallization, but also to liquid/liquid phases for emulsion application or liquid/gas for boiling systems.

6. Acknowledgments

The authors thank the support of the project WATERSAFE of the French National Research Agency (ANR-20-CE04- 0002) : "Wastewater purification by solidification : Simulation by the Phase Field method (WATERSAFE)". The authors gratefully thank Pr. Thierry Biben (ILM, University Claude Bernard Lyon1) for the fruitful scientific discussions and its help for the tuning of the simulation parameters.

Références

- [1] A. Rich, Y. Mandri, D. Mangin, R. Rivoire, S. Abderafi, C. Bebon, N. Semlali, J. Klein, T. Bounahmidi, A. Bouhaouss, S. Veessler, Sea water desalination by dynamic layer melt crystallization : Parametric study of the freezing and sweating steps, *Journal of Crystal Growth* 342 (1) (2012) 110–116. doi :10.1016/j.jcrysgro.2011.03.061.
- [2] V. Ramanuj, R. Sankaran, B. Radhakrishnan, A sharp interface model for deterministic simulation of dendrite growth, *Computational Materials Science* 169 (2019) 109097. doi :10.1016/j.commatsci.2019.109097.
- [3] I. Danaila, R. Moglan, F. Hetcht, L. M. Stéphane, A newton method with adaptive finite elements for solving phase-change problems with natural convection, *Journal of Computational Physics* 274 (2014) 826–840. doi :10.1016/j.jcp.2014.06.036.
- [4] A. Bourdillon, P. Verdin, C. Thompson, Numerical simulations of water freezing processes in cavities and cylindrical enclosures, *Applied Thermal Engineering* 75 (2015) 839–855. doi :10.1016/j.applthermaleng.2014.10.021.
- [5] T. Htira, C. Cogné, E. Gagnière, D. Mangin, Experimental study of industrial wastewater treatment by freezing, *Journal of Water Process Engineering* 23 (2018) 292–298. doi :10.1016/j.jwpe.2018.04.013.
- [6] J. W. Barrett, H. Garcke, R. Nürnberg, Numerical computations of faceted pattern formation in snow crystal growth, *Phys. Rev. E* 86 (2012) 011604. doi :10.1103/PhysRevE.86.011604.
- [7] P. M. Pavel, N. Ene, Planar solidification solution with mushy zone, *Energy Conversion and Management* 44 (18) (2003) 2977–2989. doi :10.1016/S0196-8904(03)00052-9.
- [8] J. Kelly, E. Boyer, Physical improvements to a mesoscopic cellular automaton model for three-dimensional snow crystal growth, *Cryst. Growth Des.* 14 (2014) 1392–1405. doi :10.1021/cg401862u.
- [9] Y. Dang, J. Ai, J. Dai, C. Zhai, W. Sun, Comparative study on snowflake dendrite solidification modeling using a phase-field model and by cellular automaton, *Processes* 10(11) (2022) 2337. doi :10.3390/pr10112337.
- [10] R. Kobayashi, Modeling and numerical simulations of dendritic crystal growth, *Physica D : Nonlinear Phenomena* 63 (3) (1993) 410–423. doi :10.1016/0167-2789(93)90120-P.
- [11] G. Demange, H. Zapolsky, R. Patte, M. Brunel, A phase field model for snow crystal growth in three dimensions, *npj Computational Materials* 3(1) (2017) 1–7. doi :10.1038/s41524-017-0015-1.
- [12] M. Plapp, *Multiphase Microfluidics : The Diffuse Interface Model*, Springer Vienna, Vienna, 2012, Ch. Phase-Field Models, pp. 129–175. doi :10.1007/978-3-7091-1227-4_4.
- [13] N. Moelans, B. Blanpain, P. Wollants, An introduction to phase-field modeling of microstructure evolution, *Calphad* 32 (2) (2008) 268–294. doi :10.1016/j.calphad.2007.11.003.

- [14] R. Rojas, T. Takaki, M. Ohno, A phase-field-lattice boltzmann method for modeling motion and growth of a dendrite for binary alloy solidification in the presence of melt convection, *Journal of Computational Physics* 298 (2015) 29–40. doi :10.1016/j.jcp.2015.05.045.
- [15] W. J. Boettinger, J. A. Warren, C. Beckermann, A. Karma, Phase-field simulation of solidification, *Annual Review of Materials Research* 32 (1) (2002) 163–194. doi :10.1146/annurev.matsci.32.101901.155803.
- [16] R. Tönhardt, G. Amberg, Phase-field simulation of dendritic growth in a shear flow, *Journal of Crystal Growth* 194 (3) (1998) 406–425. doi :10.1016/S0022-0248(98)00687-3.
- [17] G. Demange, H. Zapolsky, R. Patte, M. Brunel, Growth kinetics and morphology of snowflakes in supersaturated atmosphere using a three-dimensional phase-field model, *Phys. Rev. E* 96(2) (2017) 022803. doi :10.1103/PhysRevE.96.022803.
- [18] A. Karma, W.-J. Rappel, Quantitative phase-field modeling of dendritic growth in two and three dimensions, *Phys. Rev. E* 57 (1998) 4323–4349. doi :10.1103/PhysRevE.57.4323.
- [19] B. Echebarria, R. Folch, A. Karma, M. Plapp, Quantitative phase-field model of alloy solidification, *Phys. Rev. E* 70 (2004) 061604. doi :10.1103/PhysRevE.70.061604.
- [20] Q. Tan, S. A. Hosseini, A. Seidel-Morgenstern, D. Thévenin, H. Lorenz, Modeling ice crystal growth using the lattice boltzmann method, *Physics of Fluids* 34 (2022). doi :10.1063/5.0072542.
- [21] K. G. Libbrecht, Physical dynamics of ice crystal growth, *Annual Review of Materials Research* 47 (1) (2017) 271–295. doi :10.1146/annurev-matsci-070616-124135.
- [22] N. U., The formation of ice crystals, compendium of meteorology, (American Meteorological Society (1951) 207–220.
- [23] A. Shibkov, Y. Golovin, M. Zheltov, A. Korolev, A. Leonov, Morphology diagram of nonequilibrium patterns of ice crystals growing in supercooled water, *Physica A : Statistical Mechanics and its Applications* 319 (2003) 65–79. doi :10.1016/S0378-4371(02)01517-0.
- [24] H. Yuan, K. Sun, K. Wang, J. Zhang, Z. Zhang, L. Zhang, S. Li, Y. Li, Ice crystal growth in the freezing desalination process of binary water-nacl system, *Desalination* 496 (2020) 114737. doi :10.1016/j.desal.2020.114737.
- [25] R. Van der Sman, Phase field simulations of ice crystal growth in sugar solutions, *International Journal of Heat and Mass Transfer* 95 (2016) 153–161. doi :10.1016/j.ijheatmasstransfer.2015.11.089.
- [26] S.-L. Wang, R. Sekerka, Algorithms for phase field computation of the dendritic operating state at large supercoolings, *Journal of Computational Physics* 127 (0161) (1996) 110–117. doi :10.1006/jcph.1996.0161.
- [27] S.-L. Wang, R. Sekerka, A. Wheeler, B. Murray, S. Coriell, R. Braun, G. McFadden, Thermodynamically-consistent phase-field models for solidification, *Physica D : Nonlinear Phenomena* 69 (1) (1993) 189–200. doi :10.1016/0167-2789(93)90189-8.
- [28] The International Association for the Properties of Water, Steam, Revised release on the equation of state 2006 for H_2O Ice Ih, IPAWS (2009).
- [29] M. Plapp, 15- phase-field models, in : T. Nishinaga (Ed.), *Handbook of Crystal Growth* (Second Edition), second edition Edition, Elsevier, Boston, 2015, pp. 631–668. doi :10.1016/B978-0-444-56369-9.00015-0.
- [30] Y. Choi, M. R. Okos, Effects of temperature and composition on the thermal properties of foods, *Food Engineering and Process Applications* 1 (1986) 93–101.
- [31] M. Saclier, Contrôle par ultrasons de la nucléation de glace lors de la congélation en flacons : modélisation de la cinétique de nucléation et caractérisation expérimentale des cristaux, Thèse de l'Université Lyon1, 2009.
- [32] H. Callen, *Thermodynamics and an Introduction to Thermostatistics*, Wiley, 1991.
- [33] L. Gránásy, Cahn–Hilliard-type density functional calculations for homogeneous ice nucleation in undercooled water, *Journal of*

- Molecular Structure 485–486 (1999) 523–536. doi :10.1016/S0022-2860(99)00095-2.
- [34] J. W. Cahn, J. E. Hilliard, Free energy of a nonuniform system. i. interfacial free energy, *The Journal of Chemical Physics* 28 (2) (1958) 258–267. doi :10.1063/1.1744102.
- [35] W. Mullins, R. Sekerka, Stability of a planar interface during solidification of a dilute binary alloy, in : P. Pelcé (Ed.), *Dynamics of Curved Fronts*, Academic Press, San Diego, 1988, pp. 345–352. doi :10.1016/B978-0-08-092523-3.50037-X.
- [36] J. Langer, R. Sekerka, T. Fujioka, Evidence for a universal law of dendritic growth rates, *Journal of Crystal Growth* 44 (4) (1978) 414–418. doi :10.1016/0022-0248(78)90007-6.
- [37] A. Wheeler, B. Murray, R. Schaefer, Computation of dendrites using a phase field model, *Physica D : Nonlinear Phenomena* 66 (1) (1993) 243–262. doi :10.1016/0167-2789(93)90242-S.
- [38] P. Manjunatha, Curvature measure and visualization, <https://github.com/preethamam/CurvatureVisualize/releases/tag/1.0.6>, *GitHub* (2023).
- [39] G. Demange, R. Patte, H. Zapolsky, Induced side-branching in smooth and faceted dendrites : theory and phase-field simulations, *Phil. Trans. R. Soc.* 380 (2022). doi :10.1098/rsta.2020.0304.